Optics Letters

Diode-pumped Kerr-lens mode-locked Yb:$MgWO_4$ laser

Hai-Yu Nie,[1,2] Zhang-Lang Lin,[1] Pavel Loiko,[3] Huang-Jun Zeng,[1] Lizhen Zhang,[1] Zhoubin Lin,[1] Ghassen Zin Elabedine,[4] Xavier Mateos,[4] Valentin Petrov,[5] Ge Zhang,[1,6] and Weidong Chen[1,5,*]

[1]Fujian Institute of Research on the Structure of Matter, Chinese Academy of Sciences, 350002 Fuzhou, China
[2]College of Chemistry and Materials Science, Fujian Normal University, 350002 Fuzhou, China
[3]Centre de Recherche sur les Ions, les Matériaux et la Photonique (CIMAP), UMR 6252 CEA-CNRS-ENSICAEN, Université de Caen, 6 Boulevard Maréchal Juin, 14050 Caen Cedex 4, France
[4]Universitat Rovira i Virgili (URV), Física i Cristal·lografia de Materials (FiCMA), 43007 Tarragona, Spain
[5]Max Born Institute for Nonlinear Optics and Short Pulse Spectroscopy, Max-Born-Str. 2a, 12489 Berlin, Germany
[6]zhg@fjirsm.ac.cn
*chenweidong@fjirsm.ac.cn

Received 10 December 2024; revised 9 January 2025; accepted 10 January 2025; posted 13 January 2025; published 31 January 2025

We present the first Kerr-lens mode-locked solid-state laser based on ytterbium-doped monoclinic magnesium monotungstate as an active medium. The diode-pumped Yb:$MgWO_4$ laser delivers soliton pulses as short as 32 fs at 1079 nm with a pulse repetition rate of ~68 MHz via soft-aperture Kerr-lens mode-locking. To the best of our knowledge, these are the shortest pulses ever achieved from any ytterbium-doped tungstate crystals.

https://doi.org/10.1364/OL.550819

Magnesium tungstate, $MgWO_4$, a crystal called huanzalaite in the mineral form, belongs to the family of monoclinic transition-metal monotungstates (point group $2/m$, space group $P2/c$) with the general chemical formula $M^{2+}WO_4$, where M^{2+} denotes Mg^{2+}, Zn^{2+}, Mn^{2+}, Cd^{2+}, Fe^{2+}, or Ni^{2+} [1]. $MgWO_4$ is optically biaxial and exhibits high thermal conductivity (~8.7 W/mK, direction-average value [2]) and weak anisotropy of relative thermal expansion ($\alpha_a = 11.22$, $\alpha_b = 8.09$, and $\alpha_c = 8.77$ in units of 10^{-6} K^{-1} [3]). The wolframite-type structure of $MgWO_4$ consists of a network of interconnected zigzag chains formed by alternating distorted MgO_6 and WO_6 octahedra aligned along the $\boldsymbol{c}$-axis [4]. The Mg^{2+} cations are located in a single type of sites with C_2 symmetry and distorted VI-fold coordination. When $MgWO_4$ is doped with Yb^{3+} ions, they replace the Mg^{2+} ions in the structure. The charge compensation occurs through Mg^{2+} vacancies or incorporation of impurity cations with different valences into the interstitial sites. The distortion of the crystal field around the Yb^{3+} ions is enhanced by the notable difference of the ionic radii of Mg^{2+} (0.72 Å) and Yb^{3+} (0.868 Å). Yb^{3+}-doped $MgWO_4$ crystals exhibit strongly anisotropic and broadband absorption and emission characteristics. The latter is attributed to inhomogeneous spectral line broadening and strong electron–phonon interaction [5].

Crystal growth, polarized spectroscopy, and continuous-wave (CW) laser performance of Yb^{3+}-doped $MgWO_4$ had been previously systematically investigated [6,7]. Pumping with a multi-transverse-mode, high-power, fiber-coupled InGaAs laser diode at 968.5 nm, a maximum output power as high as 18.2 W was achieved at 1056 nm with a slope efficiency of 89% approaching the Stokes limit [7]. Applied as a laser gain medium for generation of optical vortex beams, a first-order Laguerre–Gaussian doughnut mode (LG_{01}) with high purity and good beam quality was selectively excited with an output power of 2.73 W at 1060.5 nm and an optical efficiency of 33.3% [8]. Employing a semiconductor saturable absorber mirror (SESAM) for passively mode-locked (ML) operation, the Yb:$MgWO_4$ laser generated soliton pulses as short as 125 fs at 1065 nm with an average output power of 20 mW at a pulse repetition rate of 117 MHz [9].

Compared to the well-known Yb^{3+}-doped monoclinic rare-earth double tungstates, Yb:$KRE(WO_4)_2$, where RE stands for Y, Gd, or Lu, Yb:$MgWO_4$ exhibits stronger crystal fields (larger Stark splitting of Yb^{3+} multiplets) leading to broader absorption and emission bands, as well as superior thermo-optical properties, which are especially advantageous for power-scalable operation at ~1 μm pumping by high-power InGaAs laser diodes near 980 nm.

The Yb:$MgWO_4$ crystal used in this work was grown by the top-seeded solution growth method using Na_2WO_4 as a solvent and 10 at.%. The charge compensation was provided by Na^+ cations entering from the flux [6]. The actual Yb^{3+} doping concentration, 1.25 at.%, was determined by inductively coupled plasma mass spectroscopy (ion density: $N_{Yb} = 1.82 \times 10^{20}$ cm^{-3}). The optical properties of Yb:$MgWO_4$ are characterized in the frame of three mutually orthogonal optical indicatrix axes, labeled following the relation for the principal refractive indices,

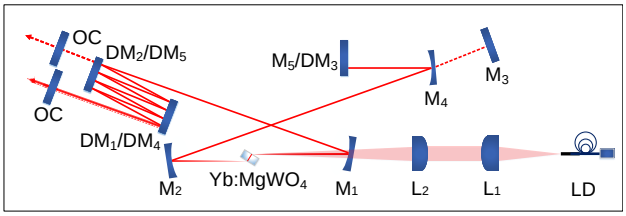

Fig. 1. Schematic of the diode-pumped Yb:$MgWO_4$ laser. LD, fiber-coupled laser diode; L_1, aspherical lens; L_2, spherical lens; M_1, M_2, and M_4, concave mirrors; M_3 and M_5, flat rear mirrors; DM_1 – DM_5, flat dispersive mirrors; OC, output coupler.

$n_p < n_m < n_g$, where $n_p = 1.981$, $n_m = 2.016$, and $n_g = 2.167$ at 1064 nm [10].

The relatively short fluorescence lifetime (366 µs) of Yb^{3+} in ions in $MgWO_4$ contributes to its ability to achieve stable ML operation, notably by minimizing Q switching instability. The large Stark splitting of the ground state ($^2F_{7/2}$) of Yb^{3+} in $MgWO_4$, which is 765 cm^{-1}, favors low-threshold and high-efficiency laser operation while reducing the temperature sensitivity [7]. These promising spectroscopic features, together with preliminary laser results, motivated us to further explore soft-aperture Kerr-lens mode-locking (KLM). Using a low-power, high-brightness laser diode as a pump source, the KLM Yb:$MgWO_4$ laser described in this Letter generates 32 fs soliton pulses (nine optical cycles) around 1 µm.

Laser operation of the Yb:$MgWO_4$ crystal was investigated in an X-folded, astigmatically compensated standing-wave cavity, as shown in Fig. 1. The laser element, a cubic N_g-cut Yb:$MgWO_4$ crystal with the dimensions of 3×3 mm^2 in aperture and 3 mm in thickness, was polished to laser-grade quality on both sides with high parallelism. It was mounted in a copper holder without active cooling and positioned between two dichroic folding mirrors (M_1 and M_2, radius of curvature, RoC = −100 mm) at Brewster's angle to minimize insertion losses. The laser polarization direction was selected by orienting the crystal for maximum laser gain, i.e., $\boldsymbol{E} \,||\, N_m$. A spatially single-mode, fiber-coupled InGaAs laser diode emitting unpolarized radiation was used as a pump source. Its emission wavelength was locked at 976 nm using a fiber Bragg grating (FBG), with a spectral linewidth of 0.2 nm (full width at half maximum, FWHM). The pump beam was collimated using an aspherical lens (L_1, focal length $f = 26$ mm) and focused into the crystal with a spherical lens (L_2, $f = 75$ mm), producing a beam waist (radii) of 14.6 µm × 32.8 µm in the sagittal and tangential planes, respectively. After passing through the imaging lenses and the pump mirror M_1, the maximum incident pump power amounted to 1.32 W, with a beam propagation factor (M^2) of 1.02.

The CW laser performance of the diode-pumped Yb:$MgWO_4$ laser was evaluated with a four-mirror cavity, as shown in Fig. 1. One arm of the cavity was terminated with a flat rear mirror (M_3), while the other arm ended with a plane-wedged output coupler (OC). The cavity mode inside the laser crystal was estimated using the ray transfer matrix (ABCD) formalism, resulting in a beam waist (radii) of 24.9 µm × 42.3 µm in the sagittal and tangential planes, respectively. The measured pump absorption under lasing conditions showed a weak dependence on the transmission of the OC (T_{OC}), which varied from 63.5% to 65.3%. The input–output characteristics of the diode-pumped Yb:$MgWO_4$ laser are shown in Fig. 2(a). Using a 7.5% OC, the maximum CW output power of 406 mW was

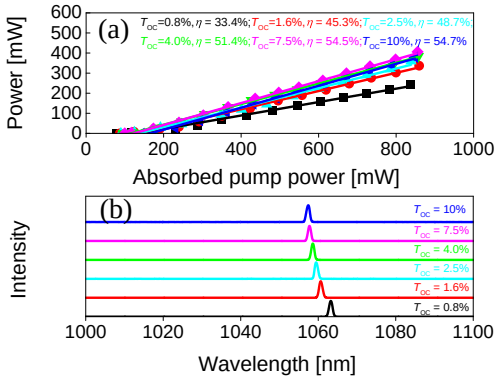

Fig. 2. Diode-pumped CW Yb:$MgWO_4$ laser: (a) power transfer curves for different OCs: η, slope efficiency; T_{OC}, OC transmission; (b) laser spectra; the laser polarization is $\boldsymbol{E} \,||\, N_m$.

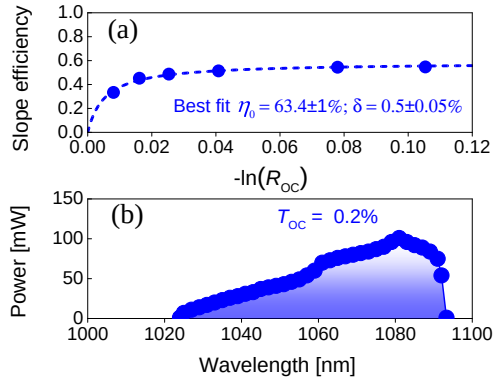

Fig. 3. Diode-pumped CW Yb:$MgWO_4$ laser: (a) Caird analysis: slope efficiency versus output coupler reflectivity, $R_{OC} = 1 - T_{OC}$; (b) spectral tuning curve with $T_{OC} = 0.2\%$.

obtained at an absorbed pump power of 855 mW, corresponding to a slope efficiency (η) of 54.5% and an optical efficiency of 47.5%. The laser threshold gradually increased with T_{OC}, from 127 mW ($T_{OC} = 0.8\%$) to 235 mW ($T_{OC} = 10\%$). The laser spectra exhibited a monotonic blueshift as T_{OC} increased, and the laser wavelength ranged from 1063.1 nm to 1057.2 nm; see Fig. 2(b). This spectral behavior is attributed to the quasi-three-level nature of the Yb laser, with inherent reabsorption loss.

The Caird analysis [11] was performed to estimate the total round trip cavity losses (δ, excluding reabsorption losses) and the intrinsic slope efficiency (η_0) by fitting the measured slope efficiency (η) as a function of the OC reflectivity, $R_{OC} = 1 - T_{OC}$, as shown in Fig. 3(a). The best fit yields an intrinsic slope efficiency (accounting for mode-matching and quantum efficiency) of $\eta_0 = 63.4 \pm 1\%$ and $\delta = 0.5 \pm 0.05\%$. The low value of δ confirms the excellent optical quality of the laser crystal. The spectral tuning of the CW diode-pumped Yb:$MgWO_4$ laser was investigated by inserting a quartz-based Lyot filter near the OC at Brewster's angle. The laser wavelength was continuously tunable from 1024 to 1093.8 nm, covering a range of ~70 nm at the zero-power level, with 1.3 W of incident power and a 0.2% OC, as shown in Fig. 3(b).

The KLM operation of the diode-pumped Yb:$MgWO_4$ laser was investigated by incorporating three flat dispersive mirrors (DMs) into the cavity, as shown in Fig. 1. Two of them were

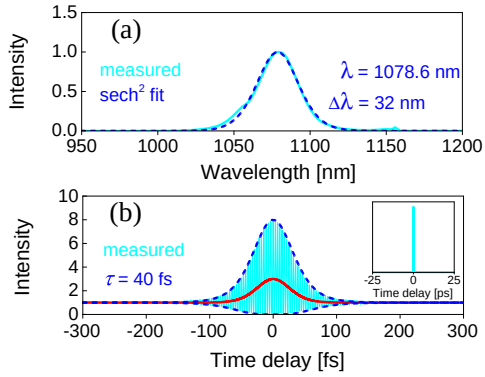

Fig. 4. Diode-pumped KLM Yb:$MgWO_4$ laser with $T_{OC} = 2.5\%$: (a) optical spectrum and (b) interferometric autocorrelation trace. Inset in (b): simultaneously measured long-scale (50 ps) autocorrelation trace. The red curve in (b) shows the intensity autocorrelation profile.

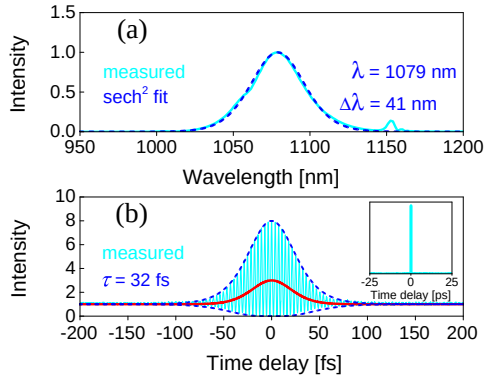

Fig. 5. Diode-pumped KLM Yb:$MgWO_4$ laser with $T_{OC} = 1.6\%$: (a) optical spectrum and (b) interferometric autocorrelation trace. Inset in (b): simultaneously measured long-scale (50 ps) autocorrelation trace. The red curve in (b) shows the intensity autocorrelation profile.

located in the cavity arm with the OC. In the other cavity arm, the flat rear mirror M_3 was replaced by an additional concave mirror M_4 (RoC = −100 mm) and a flat rear mirror M_5 or a flat DM, DM_3. Initially, a 2.5% OC was employed to evaluate the KLM performance at the maximum incident pump power of 1.32 W. The configuration utilized three bounces on DM_1 and DM_2, each with group delay dispersion (GDD) of −150 fs^2 per bounce, and one bounce on DM_3 also with a GDD of −150 fs^2 per bounce. This resulted in an overall round trip negative GDD of −1950 fs^2, which served to compensate for material dispersion and balance the self-phase modulation (SPM) induced by the Kerr nonlinearity in the laser crystal.

To discriminate the CW regime, the laser cavity of the Yb:$MgWO_4$ laser was aligned near the edge of the stability region. This was achieved by translating the folding mirror M_2 progressively away from the pump mirror M_1. This adjustment led to a significant reduction in output power, dropping down to 28 mW. The KLM operation was then initiated by gently tapping the OC or by translating the flat rear mirror DM_3. When the KLM operation regime was established, the average output power experienced a sharp increase reaching 97 mW. The characterization of the KLM performance of the Yb:$MgWO_4$ laser is shown in Fig. 4. The measured optical spectrum of the femtosecond pulses was centered at 1078.6 nm, with a spectral bandwidth of 32 nm (FWHM, assuming a $sech^2$-shaped spectral profile), as shown in Fig. 4(a). The pulse duration was estimated from the interferometric autocorrelation trace based on second-harmonic generation (SHG), as shown in Fig. 4(b), which was deconvolved to yield a pulse duration of 40 fs (FWHM), assuming a $sech^2$ temporal profile. The corresponding time-bandwidth product (TBP) of 0.330 suggested that the generated pulses were slightly chirped. Single-pulse steady-state ML operating was confirmed by a background-free intensity autocorrelation trace measured over a long time scale (50 ps), as depicted in the inset of Fig. 4(b). The pulse repetition rate was 68.6 MHz, corresponding to an optical cavity length of 2.187 m. The peak output power with this OC reached 31.1 kW. The absorbed pump power under these conditions was 802 mW.

The pulse duration could be further reduced by decreasing the total negative GDD and using lower output coupling. By replacing DM_3 with a flat dielectric mirror (M_5) with low GDD, and applying two different flat dispersive mirrors DM_4 and DM_5 (see Fig. 1), each with GDD = −100 fs^2 per bounce, the total negative GDD amounted to −1600 fs^2. With a 1.6% OC, the maximum average output power for the shortest pulses dropped to 50 mW, corresponding to an absorbed pump power of 789 mW. The measured optical spectrum exhibited a nearly $sech^2$ shape, centered at 1079 nm, with a spectral bandwidth (FWHM) of 41 nm; see Fig. 5(a).

The generation of soliton pulses as short as 32 fs was confirmed via performing an interferometric autocorrelation measurement; see Fig. 5(b). By counting the fringes in the measured autocorrelation trace, it was determined that the pulse duration corresponded to nine optical cycles. Single-pulse ML operation, free of satellite pulses, was verified by recording the non-colinear SHG intensity autocorrelation trace on a 50 ps time scale; see the inset of Fig. 5(b). The pulse repetition rate was ~68 MHz and the peak power was 20.3 kW. The TBP was calculated to be 0.338, indicating that the pulses were again somewhat chirped relative to the ideal soliton pulses, which have a Fourier-transfer-limited TBP of 0.315.

The amplitude and phase of the shortest pulses from the diode-pumped KLM Yb:$MgWO_4$ laser were retrieved using spectral phase interferometry for direct electric-field reconstruction (SPIDER); see Fig. 6(a). The spectral phase, which was reconstructed from the SPIDER trace, is presented in Fig. 6(b), along with the independently measured optical spectrum of the shortest pulses. The reconstructed temporal intensity and phase profiles of the shortest pulses are shown in Fig. 6(c). The retrieved pulse duration was found to be 32 fs (FWHM), which is in excellent agreement with the independently estimated value from the interferometric autocorrelation. The residual chirp was determined to be −58 fs^2 by fitting the phase profile of the main spectral peak.

To assess the stability of the KLM operation of the diode-pumped Yb:$MgWO_4$ laser, radio-frequency (RF) spectra were recorded for the shortest pulses. The fundamental beat note was centered at 67.99 MHz, with a very high extinction ratio of 79 dBc above the carrier; see Fig. 7(a). Such a high contrast, coupled with the measured uniform harmonics over the 1 GHz frequency span, indicates a stable single-pulse steady-state ML operation, with no evidence of Q-switching instabilities.

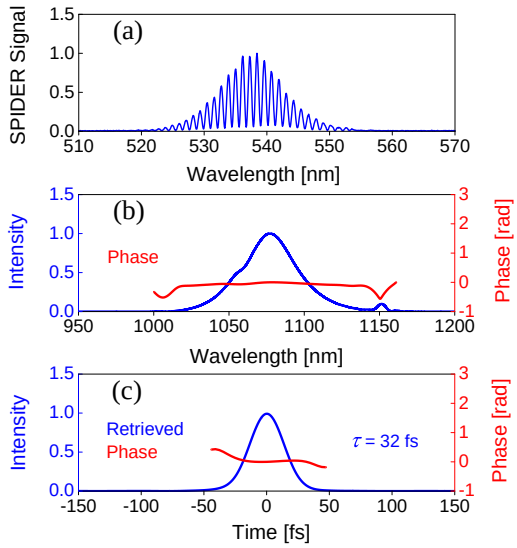

Fig. 6. SPIDER characterization of the shortest pulses from the diode-pumped KLM Yb:$MgWO_4$ with 1.6% OC: (a) SPIDER interferogram; (b) the independently measured spectrum (blue curve) together with the reconstructed spectral phase (red curve); (c) reconstructed temporal intensity (blue curve) and phase profiles (red curve).

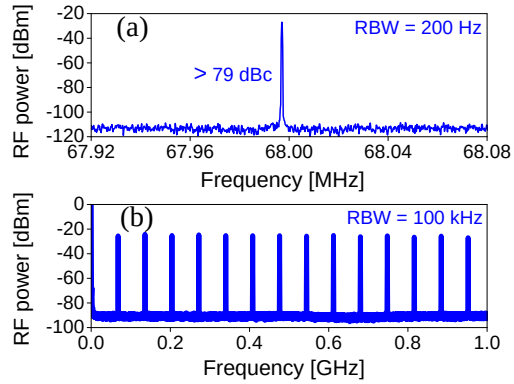

Fig. 7. RF spectra of the diode-pumped KLM Yb:$MgWO_4$ laser for the shortest pulses: (a) fundamental beat note, RBW = 200 Hz; (b) 1 GHz span with a RBW of 100 kHz. RBW, resolution bandwidth.

It is worth comparing the KLM performance of the Yb:$MgWO_4$ crystal with that of Yb^{3+}-doped monoclinic double tungstates. Liu *et al.* reported on a KLM diode-pumped Yb:$KY(WO_4)_2$ laser delivering 71 fs pulses at 1057 nm at an average output power of 120 mW [12]. To access a relatively broad electronic gain bandwidth $\Delta\lambda_g$ of 25 nm, the authors used a low-gain light polarization $\boldsymbol{E} \parallel N_p$.

The gain bandwidth of Yb^{3+} ions in $MgWO_4$ relying on electronic transitions ($\Delta\lambda_g = 15$ nm for $\boldsymbol{E} \parallel N_m$ [7]) is inferior to the value given above. To overcome this limitation, we operated the KLM laser in the low-loss / low-inversion regime shifting the laser wavelength to the long-wave part of the gain spectrum mainly determined by the exponential phonon sideband. In this case, for the spectral gain maximum of 1080 nm, one finds $\Delta\lambda_g$ ~45 nm being in line with the measured spectral bandwidth of the KLM laser. We cannot exclude strong self-phase modulation as an additional source of spectral broadening for the developed KLM laser [13].

In conclusion, we have demonstrated, to the best of our knowledge, the first Kerr-lens mode-locked operation of a diode-pumped Yb:$MgWO_4$ laser. Benefiting from its superior thermo-mechanical properties and broadband emission characteristics, soliton pulses as short as 32 fs were directly generated from the diode-pumped Yb:$MgWO_4$ laser at 1079 nm, with an average output power of 50 mW and a pulse repetition rate of ~68 MHz. This result represents the shortest pulse duration ever achieved from any Yb^{3+}-doped tungstate crystal. Furthermore, by optimizing the doping concentration of Yb^{3+} ions in the $MgWO_4$ crystal, power scaling of the Yb:$MgWO_4$ mode-locked laser could be achieved while maintaining the same pulse duration level. This could be expected by using high-power and high-brightness Yb fiber lasers as pump sources.

Funding. National Natural Science Foundation of China (62475263); Science and Technology Projects of Fujian Province (2024I0041, 2023H0047); Sino-German Scientist Cooperation and Exchanges Mobility Program (M-0040); MICIU/AEI;/ ; FEDER/UE (PID2022-141499OB-10).

Acknowledgment. Xavier Mateos acknowledges the Serra Húnter program.

Disclosures. The authors declare no conflicts of interest

Data availability. Data underlying the results presented in this paper are not publicly available at this time but may be obtained from the authors upon reasonable request.

REFERENCES

1. E. Cavalli, A. Belletti, and M. G. Brik, J. Phys. Chem. Solids **69**, 29 (2008).
2. L. Zhang, Y. Huang, S. Sun, *et al.*, J. Lumin. **169**, 161 (2016).
3. L. Zhang, P. Loiko, J. M. Serres, *et al.*, J. Lumin. **213**, 316 (2019).
4. P. Becker, L. Bohatý, H. J. Eichler, *et al.*, Laser Phys. Lett. **4**, 884 (2007).
5. P. Loiko, L. Zhang, J. M. Serres, *et al.*, J. Alloys Compd. **763**, 581 (2018).
6. L. Zhang, W. Chen, J. Lu, *et al.*, Opt. Mater. Express **6**, 1627 (2016).
7. P. Loiko, M. Chen, J. M. Serres, *et al.*, Opt. Lett. **45**, 1770 (2020).
8. J. Lu, H. Lin, G. Zhang, *et al.*, Laser Phys. Lett. **14**, 085807 (2017).
9. H. Lin, G. Zhang, L. Zhang, *et al.*, Opt. Express **25**, 11827 (2017).
10. K. A. Subbotin, Y. I. Zimina, K. V. Kuleshova, *et al.*, in *International Conference Laser Optics (ICLO)* (IEEE, 2022), P. ThR1-p38.
11. J. A. Caird, S. A. Payne, P. R. Staber, *et al.*, IEEE J. Quantum Electron. **24**, 1077 (1988).
12. H. Liu, J. Nees, and G. Mourou, Opt. Lett. **26**, 1723 (2001).
13. J. Drs, J. Fischer, N. Modsching, *et al.*, Opt. Express **29**, 35929 (2021).